# Dual-band Artificial Magnetic Conductor

**Julien Sarrazin*, Anne Claire Lepage, and Xavier Begaud**

Institut Telecom, Telecom ParisTech - LTCI CNRS UMR 5141, Paris, France
*corresponding author, E-mail: julien.sarrazin@telecom-paristech.fr

## Abstract

A dual-band Artificial Magnetic Conductor (AMC) is presented in this paper. The proposed metasurface is based on a spiral geometry in which an additional resonance has been introduced thanks to a physical understanding of the structure's behavior. The design is compact and the two frequency bands can be adjusted independently. Furthermore, an analytical model is developed which can predict both the frequencies at which the metasurface reflects incident waves in-phase.

## 1. Introduction

Metasurfaces such as High Impedance Surfaces (HIS) have a great potential regarding antenna applications [1]. These surfaces can exhibit two interesting properties. One is an Electromagnetic Band Gap (EBG) which forbids the propagation of surface waves. This property can help in reducing the mutual coupling between different antennas of an array for example. The second one is the in-phase reflection of incident waves that makes the metasurface behaving like an Artificial Magnetic Conductor (AMC). This second property allows locating such a metasurface close to an antenna in order to enhance its directivity by acting as a reflector.

AMC metasurfaces are resonant surfaces composed of printed unit-cells over a grounded dielectric slab. So the in-phase reflection of incident waves is achieved only about their resonance frequency. However, antennas are frequently operating at different frequencies simultaneously. Consequently, multi-band AMC are required.

Dual-band behavior can be obtained using two or more layers of metallic printed patterns [2, 3], or using lumped components [4, 5]. However, both these approaches increase the cost of the AMC. Thus, several uni-planar designs have been proposed in order to achieve either dual-band [6-11] or multi-band characteristics [12]. However, these surfaces are not easy to design because their frequency bands cannot be adjusted independently. In [13], a simple dual-band design based on a square patch and a slot is proposed for which two frequency bands can be adjusted independently. However, the unit-cell is relatively large and comparable to the size of a wideband monopole antenna [13]. This may be a problem especially if the surface available for the AMC is not large. A compact unit-cell design insures that a sufficient number of unit-cells can be located over a limited size surface in order to produce an in-phase reflection.

In this paper, a new dual-band AMC based on a spiral pattern is introduced. The proposed design is uni-planar and does not contain any vias in order to obtain an inexpensive and easy-to-fabricate structure. Each band can be tuned independently and to facilitate the design, an analytical model is given which can predict the resonance frequency of both the bands. Section 2 presents the spiral-based single-band AMC along with analytic formulae. In section 3, an additional resonance is introduced to achieve the dual-band behavior and the related analytical model is given. In section 4, a dual-band GPS application is considered and related designing issues are discussed. Finally, a conclusion is drawn in section 5.

## 2. Single-band AMC

### 2.1. Design

The proposed structure is based on a spiral unit-cell introduced in [14] which presents the advantage to be compact while exhibiting a bandwidth similar to other bigger patterns [15]. However, unlike in [14], the spiral used here does not contain any metallic vias and the structure is consequently similar to the one found in [16]. A quarter of the unit-cell is presented in figure 1. To obtain the complete unit-cell, the spiral has to be mirror duplicated along *x*- and *y*-axis. The metallic pattern is constructed with the geometrical parameters $l_{spir}$ and $g$. $g$ is the gap between spiral's arms and $l_{spir}$ is related to the gap $g$ and the width of spiral's arms $w_{CPW}$ with:

$$l_{spir} = w_{CPW} + g \qquad (1)$$

So the length of this quarter unit-cell is $8l_{spir}$. The spiral is printed on a grounded dielectric slab. In figure 1, the grounded dielectric slab is actually composed of two dielectric layers of thickness $h_1$, $h_2$ and relative permittivity $\varepsilon_{r1}$, $\varepsilon_{r2}$, respectively. Only the lower layer ($h_1$, $\varepsilon_{r1}$) has a ground plane. Two layers are taken into account in order to consider the following scenario. The upper layer is a dielectric substrate, necessary for the spiral to be printed, whereas the lower layer is only vacuum (which in practice can be foam or honeycomb structure). This vacuum layer is useful in order to increase the thickness of the structure, and so the AMC bandwidth, without increasing significantly neither the weight nor the losses.

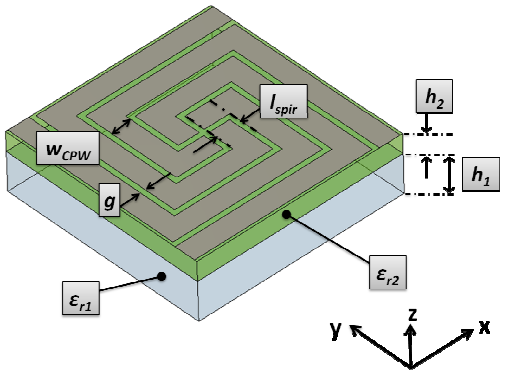


Figure 1: Single-band spiral AMC quarter unit-cell.

### 2.2. Analytical Modeling

In order to obtain a dual-band AMC, it is necessary to add a second resonance to the metasurface. To do so, we firstly analyze the resonance phenomenon involved in the spiral. The figure 2 presents the full spiral unit-cell. At the frequency for which the surface behaves like an AMC (i.e. when the reflected phase is null), a resonance occurs. A stationary wave is established in the split strip presented in blue color in figure 2 (the incident electric field is considered polarized along *x*-axis). This strip supports a coplanar waveguide (CPW)-like quasi-TEM mode of propagation with grey lines being its ground plane. Yellow lines are parts of the neighbor resonating strips. Note that when the electric field is polarized along *y*-axis, resonating strips become the ground plane and vice versa. So the structure is equivalent to a CPW stepped-impedance dipole. Consequently, its resonance frequency can be analytically determined.

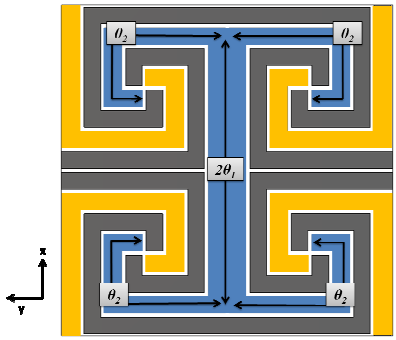


Figure 2: CPW stepped-impedance dipole identification.

By considering the first mode of a stepped-impedance resonator, resonance conditions are satisfied when [17]:

$$\tan(\theta_1)\tan(\theta_2) = R_z \qquad (2)$$

where $\theta_1$ et $\theta_2$ are the electrical lengths showed in figure 2 and equal to:

$$\theta_1 = \beta_1 l_1 = \frac{\omega}{c}\sqrt{\varepsilon_{reff1}}.l_1 \qquad (3)$$

$$\theta_2 = \beta_2 l_2 = \frac{\omega}{c}\sqrt{\varepsilon_{reff2}}.l_2 \qquad (4)$$

with $\omega$ the angular frequency, $c$ the light velocity, $l_1 = 6.5l_{spir}$ and $l_2 = 9.5l_{spir} - g/2$. $R_z$ is the ratio between the characteristic impedance $Z_2$ of the dipole's part whose line length is $\theta_2$ and width $W_{CPW2} = l_{spir}$-$g$ and the characteristic impedance $Z_1$ of the part of length $\theta_1$ and line width $W_{CPW1} = 2l_{spir}$-$g$. So the impedance ratio is equal to:

$$R_z = \frac{Z_2}{2Z_1} \qquad (5)$$

Consequently, by determining $R_z$ and the effective permittivity of each part of the dipole, the resonance frequency can be found by solving equation (2).

Characteristics of a multilayered substrate conductor-backed CPW can be determined with conformal mapping [18, 19] by assuming a propagating quasi-static TEM mode. Thus, the effective permittivity can be calculated using the following set of equations:

$$\varepsilon_{reff} = 1 + q_1\varepsilon_{r1} + q_2(\varepsilon_{r2} - \varepsilon_{r1}) \qquad (6)$$

$$q_i = \frac{1}{2}\frac{K(k_i)}{K(k_i')}\frac{K(k_0')}{K(k_0)} \qquad (7)$$

where $K$ is the complete elliptic integral of the first kind and:

$$k_0 = \frac{a}{b} \qquad (8)$$

$$k_1 = \frac{\tanh\left(\frac{\pi a}{2(h_1+h_2)}\right)}{\tanh\left(\frac{\pi b}{2(h_1+h_2)}\right)} \qquad (9)$$

$$k_2 = \frac{\sinh\left(\frac{\pi a}{2h_2}\right)}{\sinh\left(\frac{\pi b}{2h_2}\right)} \qquad (10)$$

$$k_i' = \sqrt{1-k_i^2} \qquad (11)$$

$$a = \frac{w_{CPW}}{2} \qquad (12)$$

$$b = \frac{w_{CPW}}{2} + g \qquad (13)$$

To obtain the value of $R_z$ from equation (5), impedances $Z_1$ and $Z_2$ are determined with:

$$Z = \frac{1}{c\sqrt{\varepsilon_{reff}}C_0} \qquad (14)$$

$$C_0 = 2\varepsilon_0\left(\frac{K(k_0)}{K(k_0')} + \frac{K(k_1)}{K(k_1')}\right) \qquad (15)$$

### 2.3. Numerical validation

To validate the proposed model, an example of spiral using no substrate but vacuum is firstly considered (so $\varepsilon_{r1} = \varepsilon_{r2} = 1$). Dimensions are $(h_1 + h_2) = 4.73$ mm and $g = 0.4$ mm. $l_{spir}$ value ranges from 1.1 mm up to 4.7 mm.

The AMC behavior occurs when the CPW stepped-impedance dipole resonates. This resonance frequency is determined analytically by solving equation (5) and results are compared with those obtained from a full-wave-analysis with the frequency domain solver of CST Microwave Studio. From full-wave-analysis, the frequency at which the reflected phase is null in the AMC's plane is determined following the procedure described in [20]. Results are shown in figure 3. As expected, it is observed that when the size of the spiral increases (i.e. when $l_{spir}$ increases), the null phase frequency decreases. Also, analytical and full-wave results are in good agreement, except when $l_{spir}$ is small and so the null phase frequency is high. This can be explained by the fact that the analytical model supposes a quasi-static TEM mode of propagation. This assumption is valid as long as the substrate thickness is small compared to the wavelength. When the operating frequency increases, the thickness $h_1 + h_2$ becomes larger with respect to the wavelength. Nevertheless, for the given example, the model gives quite accurate results for frequencies below 2 GHz, even though the finite ground plane size, bends, open-end discontinuities and the coupling between the neighbor dipoles are not taken into account.

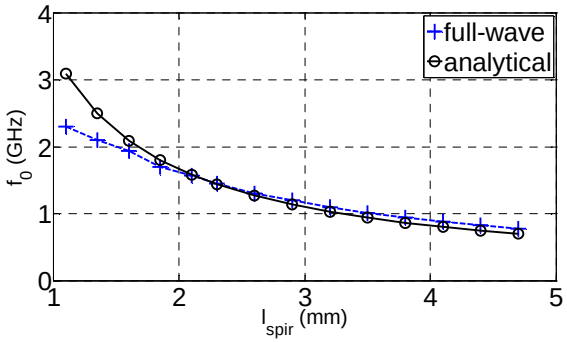


Figure 3: Influence of the spiral size (through parameter $l_{spir}$) on the null phase frequency ($\varepsilon_{r1} = \varepsilon_{r2} = 1$, $(h_1 + h_2) = 4.73$ mm, $g = 0.4$ mm).

As a second example, the presence of a dielectric layer is now considered. Dimensions are the same as previously except that $l_{spir}$ is kept constant at 2.1 mm, $h_1$= 3.15 mm and $h_2$ = 1.58 mm. The effect of the relative permittivity $\varepsilon_{r2}$ is investigated and its value ranges from 1 up to 9. Analytical and full-wave results are shown in figure 4. One can notice that the null phase frequency decreases from 1.57 GHz down to 0.75 GHz (from full-wave results) as the permittivity increases from 1 up to 9. When $\varepsilon_{r2} = 1$, analytical and full-wave results are in good agreement. However, the error increases as the permittivity increases, reaching about 11% when $\varepsilon_{r2} = 9$. It appears that, in the given example, the analytical model is more accurate for lower permittivity values. This may be explained by the fact that the higher the permittivity, the more the field is concentrated in the dielectric, thereby inducing more dispersion which is not taken into account in the analytical model.

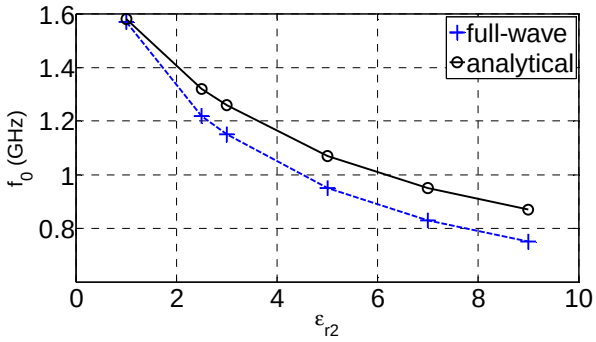


Figure 4: Influence of the relative permittivity $\varepsilon_{r2}$ on the null phase frequency ($\varepsilon_{r1} = 1$, $h_1 = 3.15$ mm, $h_2 = 1.58$ mm, $g = 0.4$ mm, $l_{spir} = 2.1$ mm).

## 3. Dual-Band AMC

### 3.1. Design and concept

The proposed dual-band geometry is presented in figure 5. Because of its symmetry, only a quarter of the structure is shown. Knowing that the current circulating along a CPW is mainly concentrated along line edges, a slot can be etched in the middle of the CPW without disturbing too much the propagation along it. By doing so, the slot creates an additional propagation structure: a Coplanar Strip Line (CPS) of gap value $w_{CPS}$. This structure, being short-circuited at one end and open-circuited at the other end, introduces an additional resonance when its equivalent length ($l_{CPS}$) is equal to a quarter of guided wavelength. So by adjusting the length of the slot, it is possible to adjust the resonance frequency of the CPS while keeping unchanged the resonance frequency of the CPW.

To validate the concept, full-wave simulations are performed with CST Microwave Studio using the following properties: $\varepsilon_{r1} = \varepsilon_{r2} = 1$, $(h_1+h_2) = 4.73$ mm, $g = 0.4$ mm, $w_{CPS} = 0.2$ mm, $l_{spir} = 2.1$ mm and $l_{CPS}$ varies from 26.75 mm up to 33.4 mm, which is the longest possible CPS length. At this value, the physical CPS length is equal to the physical CPW length ($l_{CPS} = l_1 + l_2$). Reflection phase results are shown in Figure 6. One can observe that the reflection becomes null twice over the frequency band of interest. At the lower frequency, the resonance is due to the CPW stepped-impedance dipole. At the upper frequency, the resonance is due to the CPS and so the frequency changes significantly for different values of $l_{CPS}$. Thus, two different null reflected phase frequencies can be adjusted independently which is highly suitable for dual-band designing.

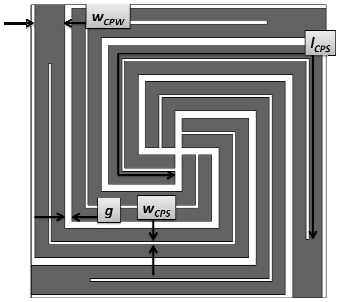


Figure 5: Dual-band spiral AMC quarter unit-cell.

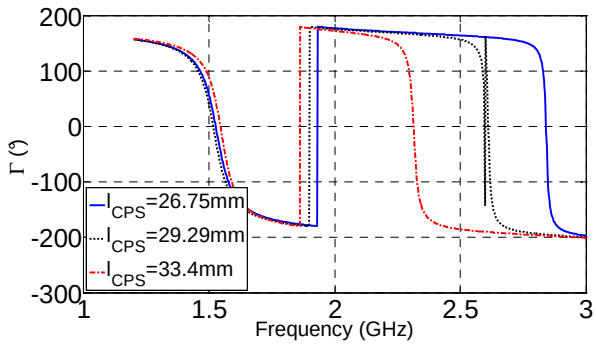


Figure 6: Reflection phase full-wave simulation results: influence of $l_{CPS}$ ($\varepsilon_{r1} = \varepsilon_{r2} = 1$, $(h_1+h_2) = 4.73$ mm, $g = 0.4$ mm, $w_{CPS} = 0.2$ mm, $l_{spir} = 2.1$ mm).

### 3.2. Analytical Modeling

Considering the quarter-wavelength resonance of the CPS, the resonance frequency is thereby given by:

$$f_0^{CPS} = \frac{c}{4 l_{CPS} \sqrt{\varepsilon_{reff}}} \tag{16}$$

By again performing a conformal mapping based on a quasi-static TEM mode assumption and by neglecting the presence of the lower ground plane, the effective permittivity of the CPS can be determined by [18]:

$$\varepsilon_{reff} = 1 + \frac{(\varepsilon_{r2} - 1)}{2} \frac{K(k_0)}{K(k_0')} \frac{K(k_2')}{K(k_2)} \tag{17}$$

using same parameters than previously except that:

$$a = \frac{w_{CPS}}{2} \tag{18}$$

$$b = \frac{W_{CPW}}{2} = \frac{l_{spir} - g}{2} \tag{19}$$

### 3.3. Numerical validation

The accuracy of the proposed CPS model is studied by taking an example similar to the previous one with a vacuum substrate ($\varepsilon_{r1} = \varepsilon_{r2} = 1$) and the following dimensions are: $(h_1+h_2) = 4.73$ mm, $l_{spir} = 2.1$ mm, $g = 0.4$ mm and $w_{CPS} = 0.2$ mm. $l_{CPS}$ varies from 25.75 mm up to 33.4 mm, which is the longest possible CPS length.

Analytical results obtained from equation (16) are compared with a full-wave analysis in figure 7. The model and the full-wave analysis results are in good agreement although the lower ground plane is not taken into account. The gap $w_{CPS}$ being narrow, the electromagnetic field is largely concentrated in its proximity and so the lower ground plane has little influence on the propagating mode.

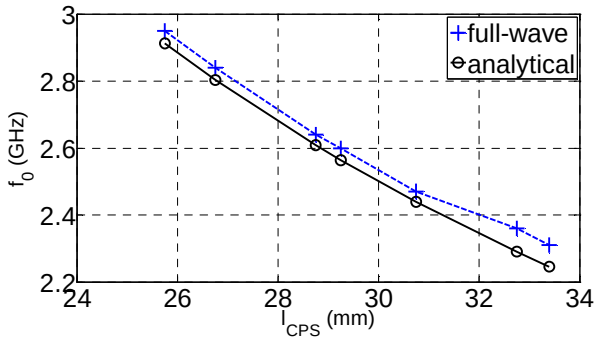


Figure 7: Influence of the CPS length (through parameter $l_{CPS}$) on the CPS null phase frequency ($\varepsilon_{r1} = \varepsilon_{r2} = 1$, $(h_1+h_2) = 4.73$ mm, $g = 0.4$ mm, $w_{CPS} = 0.2$ mm, $l_{spir} = 2.1$ mm).

The second example considers the presence of a dielectric layer. Dimensions are the same than previously except that $l_{CPS}$ is now equal to 26.75 mm, $h_1 = 3.15$ mm and $h_2 = 1.58$ mm. The effect of the relative permittivity $\varepsilon_{r2}$ is investigated and its value ranges from 1 up to 9. Analytical model is compared to full-wave analysis in figure 8. The null phase frequency decreases from 2.84 GHz down to 1.3 GHz as the permittivity increases from 1 up to 9. Results are in very good agreement. Since the CPS's gap $w_{CPS}$ is small with respect to the wavelength, the quasi-static TEM mode assumption is largely satisfied.

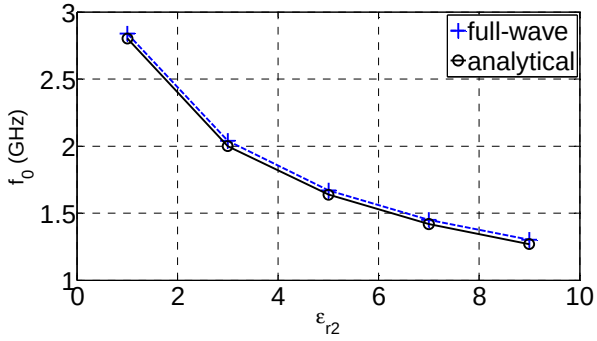


Figure 8: Influence of the relative permittivity $\varepsilon_{r2}$ on the CPS null phase frequency ($\varepsilon_{r1} = 1$, $h_1 = 3.15$ mm, $h_2 = 1.58$ mm, $g = 0.4$ mm, $w_{CPS} = 0.2$ mm, $l_{spir} = 2.1$ mm, $l_{CPS} = 26.75$ mm).

## 4. Design Considerations

In some dual-band applications, the two operating frequencies are relatively close to each other. For instance, GPS operating bands $L_1$ and $L_2$ are centered on 1.57 GHz and 1.22 GHz, respectively. Designing a wideband AMC able to cover the upper and the lower bands simultaneously is challenging [4] and may lead to very thick metasurfaces. Thus, dual-band AMCs appear to be a possible solution. However, regarding this application, a ratio $f_u/f_l = 1.28$ between upper and lower frequencies is required. Such a low ratio is not easy to obtain with conventional dual-band AMC. Even with our proposed design where two distinct propagating structures can resonate, it can be observed, from previous sections, that this ratio may be difficult to obtain. For instance, by comparing the CPW resonance frequency obtained for $l_{spir} = 2.1$ mm in figure 3 (i.e. 1.57 GHz) and the CPS one obtained in figure 7 for the maximum slot length (i.e. 2.31 GHz), the ratio $f_u/f_l$ reaches a value of 1.47. That is why an additional degree of freedom available within the structure is now investigated: the gap $g$. Its influence on the effective permittivity of each line can be simply and efficiently investigated with analytical models previously developed.

According to figure 1, a vacuum layer with a thickness $h_1 = 3.15$ mm and a substrate of permittivity $\varepsilon_{r2} = 2.5$ with a thickness $h_2 = 1.58$ mm is considered. Design parameters have following values: $l_{spir} = 2.3$ mm, $l_{CPS} = 35.3$ mm (this is the maximum possible value for which $l_{CPS} = l_1 + l_2$) and $w_{CPS} = 2.3$ mm. Results regarding the resonance frequencies of CPW and CPS lines are shown in figure 9. The gap $g$ has no significant influence on the CPS's resonance. However, when $g$ increases, the CPW's resonance frequency increases too and so the ratio $f_u/f_l$ decreases. Consequently, the parameter $g$ can be used to adjust the CPW resonance frequency, within the limit of the structure (the CPW width $W_{CPW}$ and gap $g$ are related through equation (1): when $g$ increases, $W_{CPW}$ decreases). For $g = 1$ mm, the upper frequency (CPS) is 1.625 GHz and the lower one (CPW) is 1.265 GHz. So a ratio $f_u/f_l = 1.28$ is achieved.

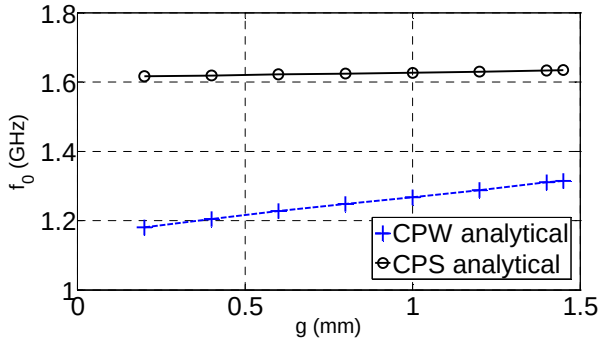


Figure 9: Influence of the gap $g$ on the CPW and CPS null phase frequency ($\varepsilon_{r1} = \varepsilon_{r2} = 1$, $(h_1+h_2) = 4.73$ mm, $l_{spir} = 2.3$ mm, $l_{CPS} = 35.3$ mm).

Finally, taking into account previous comments, a final AMC is designed and simulated in CST Microwave Studio. After optimization, the following parameter values are found: $\varepsilon_{r1} = 1$, $\varepsilon_{r2} = 2.5$, $h_1 = 3.15$ mm, $h_2 = 1.58$ mm, $l_{spir} = 2.3$ mm, $l_{CPS} = 35.3$ mm, $g = 1.45$ mm, $w_{CPS} = 0.2$ mm. The obtained reflected phase is shown in figure 10. Null phase frequencies occur at 1.26 GHz and 1.61 GHz and so exhibit a ratio $f_u/f_l = 1.28$. The bandwidth defined with the +/-90° criteria on the reflected phase [1] are:

- lower-band: $\Delta_f = 4.3$ MHz (3.4%)
- upper-band: $\Delta_f = 1.13$ MHz (0.7%)

The lower band can cover the $L_2$ bandwidth (1.7 %); however the upper band cannot cover the $L_1$ bandwidth (1.5 %). Consequently further efforts should be done in order to increase this bandwidth.

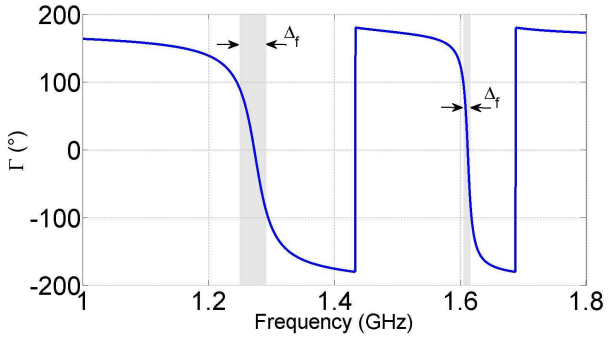


Figure 10: Dual-band AMC: reflection phase full-wave simulation results ($\varepsilon_{r1} = 1$, $\varepsilon_{r2} = 2.5$, $h_1 = 3.15$ mm, $h_2 = 1.58$ mm, $l_{spir} = 2.3$ mm, $l_{CPS} = 35.3$ mm, $g = 1.45$ mm, $w_{CPS} = 0.2$ mm).

## 5. Conclusions

In this paper, a new dual-band Artificial Magnetic Conductor (AMC) has been introduced. It has been shown that the two operating frequencies at which this AMC reflects incident waves in-phase can be set independently, which largely facilitates the designing process.

Based on a compact modified spiral pattern, the proposed AMC takes benefit of two different resonances involved within the structure. We have identified that one resonance takes place in a coplanar waveguide (CPW)-like structure whereas the other one occurs in a coplanar stripline (CPS)-like structure. Thanks to this identification, an analytical model based on conformal mapping has been developed. The model is able to predict with accuracy the null phase frequency of both bands under quasi-static assumption. Results obtained by the model have been validated with a commercial full-wave analysis software. Finally, it has been proved that the proposed design is capable of working on two bands close to each other, with a ratio $f_u/f_l = 1.28$ between upper and lower frequencies. These

results along with the analytical expressions make the proposed AMC an easy-to-design and versatile metasurface.

## Acknowledgements

The research leading to these results has received funding from the European Defence Agency (EDA) under grant agreement MIMiCRA (*Metamaterial Inspired Microwave Conformal Radar Antennas*).

## References

[1] D. Sievenpiper, *et Al.*, "High-Impedance Electromagnetic Surfaces with a Forbidden Frequency Band", *IEEE Trans. on Microwave Theory and Tech.*, vol. 47, no. 11, pp. 2059–2074, 1999.

[2] H.J. Lee, K.L. Ford, and R.J. Langley, "Dual band tunable EBG", *Electronics Letters* , vol. 44, no. 6, pp. 392-393, March 2008.

[3] J.H. Yoon, E.Y. Kim, Y. Lim, and Y.J. Yoon, "Equivalent circuit model and reflection phase control methods for dual-band AMC", *EUCAP Conference*, pp. 1222-1226, April 2011.

[4] M. Pigeon, C. Morlaas, and H. Aubert, "A Dual-band High Impedance Surface mounted with a spiral antenna for GNSS applications", *IEEE APWC Conference* pp. 994-997, Sept. 2011.

[5] M.G. Bray and D.H. Werner, "A novel design approach for an independently tunable dual-band EBG AMC surface", IEEE APS Symposium, vol. 1, pp. 289-292, June 2004.

[6] W. Wang, X.Y. Cao, R. Wang, and J.J. Ma, "A Small Dual-band EBG Structure for Microwave", *ICMMT Conference*, pp. 1637-1639, April 2008.

[7] N. Chahat, M. Zhadobov, R. Sauleau, and K. Mahdjoubi, "Improvement of the on-body performance of a dual-band textile antenna using an EBG structure", *LAPC Conference,* pp. 465-468, Nov. 2010.

[8] X. Chen, C.H. Liang, L. Liang, and Z.J. Su, "A low profile dual-band inverted L antenna with slotted electromagnetic band-gap (EBG) structures", *Int. Work. on Metamaterials*, pp. 341-343, Nov. 2008.

[9] L. Qi, H.M. Salgado, A.M. Moura, and J.R. Pereira, "Dual-band antenna design using an EBG Artificial Magnetic Conductor ground plane", *LAPC Conference*, pp. 217-220, March 2008.

[10] O. Folayan and R. Langley, "Compact EBG antenna", *EuCAP Conference*, pp. 1-4, Nov. 2006.

[11] H.H. Xie, Y.C. Jiao, K. Song, and Z. Zhang, "A Novel Multi-Band Electromagnetic Band-Gap Structure", *PIERS*, vol. 9, pp. 67-74, 2009.

[12] D.J. Kern, D.H. Werner, A. Monorchio, L. Lanuzza, and M.J. Wilhelm, "The design synthesis of multiband artificial magnetic conductors using high impedance frequency selective surfaces", *IEEE Trans. on Ant. and Propa.*, vol. 53, no. 1, pp. 8- 17, Jan. 2005.

[13] N.A. Abbasi and R. Langley, "A wideband printed monopole antenna over dual-band AMC", *LAPC conference*, pp. 221-224, Nov. 2010.

[14] Q. R. Zheng, Y. Q. Fu, and N. C. Yuan, "A Novel Compact Spiral Electromagnetic Band-Gap (EBG) Structure", *IEEE Trans. on Ant. and Propag.*, vol. 56, no. 6, pp. 1656–1660, 2006.

[15] F. Costa, S. Genovesi, and A. Monorchio, "On the bandwidth of printed frequency selective surfaces for designing high impedance surfaces", *IEEE Ant. Propag. Symp. 2009*, pp. 1-4, June 2009.

[16] L. Mouffok, *et Al.* "Mutual coupling reduction between dual polarized microstrip patch antennas using compact spiral artificial magnetic conductor", *EUCAP conference*, 902-912, 2011.

[17] M. Makimoto, and S. Yamashita, "Bandpass Filters Using Parallel Coupled Stripline Stepped Imepdance Resonators", *IEEE Trans. on Microwave Theory and Tech.*, vol. 28, no. 12, pp. 1413–1417, 1980.

[18] R.N. Simons, "Coplanar Waveguide Circuits, Components, and Systems", *John Wiley & Sons*, 2001

[19] E. Carlsson, and S. Gevorgian, "Conformal Mapping of the Field and Charge Distributions in Multilayered Substrate CPW's", *IEEE Trans. on Microwave Theory and Tech.*, vol. 47, no. 8, pp. 1544–1552, Aug. 1999.

[20] Y. Zhang, J. von Hagen, M.Younis, C. Fischer, and W. Wiesbeck "Planar Artificial Magnetic Conductors and Patch Antennas", *IEEE Trans. on Ant. and Propag.*, vol. 51, no. 10, pp. 2704-2712, Oct. 2003.